PONTIFICIA UNIVERSIDAD CATÓLICA DEL PERÚ

FACULTAD DE CIENCIAS E INGENIERÍA

"Feasibility study of the reverberant shear wave elastography technique for diabetic foot characterization

TRABAJO DE INVESTIGACIÓN PARA LA OBTENCIÓN DEL GRADO DE BACHILLER EN CIENCIAS CON MENCIÓN EN INGENIERÍA ELECTRÓNICA

AUTOR

Fernando Ivan Gutierrez Delgado

ASESORES:

Benjamín Castañeda, PhD.

MSc. Stefano Romero.

Lima, Agosto 2020

Abstract

The diabetic foot is a complication that stems from diabetes when it is not properly managed. The underlying biomechanical changes that occur inside the plantar tissue as a result of glycation when a person begins to develop this complication suggest that there is a change in its elasticity and hardness. Consequently, these changes could be estimated quantitatively with elastography, which comprises many modalities that can be implemented with a magnetic resonator, an ultrasound equipment, among other devices. One of these modalities relies on the generation of a reverberant shear wave field inside the tissue or medium of interest, called reverberant shear wave elastography (RSWE). In that sense, the literature is scarce pertaining diabetic foot research with ultrasound elastography, while the RSWE modality is still in its early stages.

The main objective of this work focuses on assessing the clinical application feasibility of this novel elastography technique by characterizing the elasticity of regions of the foot plant.

Contents

List of Figures

List of Tables

Chapter 1

1 The Problem of the Diabetic Foot and Elastography Review

1.1 The Problem of the Diabetic Foot

1.1.1 Diabetes

Diabetes mellitus (DM) describes a group of diseases characterized by chronic hyperglycemia [1]. The most known types of diabetes are type 1, an autoimmune disease characterized by the body's inability to secrete insulin; and type 2, characterized by insulin deficiency and resistance [2]. Between these two, type 2 is by far the most common type [3].

1.1.2 Statistics of Diabetes

DM is considered a worldwide epidemic [4]. For instance, in 2015, the prevalence of diabetes was estimated to be 11.6% in China [5]. In Peru, DM was number six in disease burden in 2016 [6]. In 2014, 4.9 million people died from diabetes related issues [7] and 387 million people were suffering from it [6]. This number increased to 451 million for 2017 and is estimated that it will rise to 693 million for 2045 [1].

1.1.3 Complications

DM can seriously damage the kidneys, liver, heart, eyes, neural tissue, musculoskeletal system, digestive system, can affect mental health and cognitive functioning [8]. Moreover, a serious complication that results from diabetes is the diabetic foot (DF) [4].

1.1.4 The diabetic foot

DF references the foot of a diabetic person at risk of developing pathologies such as neuropathy, peripheral vascular disease, ischemia, osteomyelitis and ulceration, among others [9]. Close to 50% of people with type 2 diabetes have neuropathy and could present complications on their feet [10][11]. This condition is a major health problem with great morbidity and mortality that can severely compromise a person's quality of life [12][13].

1.1.5 Diabetic foot ulceration

Diabetic foot ulceration (DFU) is a pathology set off by a lesion or trauma [10]. The risk of ulceration can be as high as 30% in people with DM [11]. It could lead to a more complicated problem: the amputation of the foot, which is its ultimate repercussion. This problem is often preceded by ulceration, being the precursor of 85% of them [9][12]. Once the foot ulcerates,

the risk of amputation becomes 10 to 30 times greater than in non-diabetic people. This fact is concerning because it presents a mortality follow-up as high as 80% in one to five years. Besides, amputation brings psychological, social and financial repercussions [4]. Table 1.1 shows prevalence results from numerous studies on DFU.

Table 1.1. DFU prevalence statistics shown in 5 locations, as well as worldwide.

Location	Prevalence	Year Reported	Source
Worldwide	6.30%	2017	[14]
England	7.60%	2008	[15]
United States	14%	2018	[16]
China	4.10%	2017	[14]
Sudan	18.10%	2017	[17]
France	5.60%	2017	[14]

1.1.6 Social and economic Impact

Amputation has devastating consequences as It creates a set of dire circumstances which deeply affects people from a psychological standpoint and hinders all aspects of their lives [18]. On the other hand, it is necessary to mention its economic impact. In 2017, the average cost of DF per patient was $8659 and had a total cost ranging from 9-13 billion dollars in the United States [14].

1.1.7 Biomechanical Changes of the foot

The plantar soft tissue structures contain fatty cells that absorb the initial impact created during gait [19]. Research identifies changes at a molecular level as a consequence of DM [20]. These histological changes occur as a result of glycation and compromise the structure and biomechanical properties of such tissue [19][21], which becomes unable to bear typical

mechanical loading and ultimately break down [22]. Consequently, plantar soft tissue becomes stiffer, harder, thicker [23] and unable to uniformly distribute loads [24]. This effect leads to an increase in loading [21] and combined with the inability to recognize mechanical trauma, largely because of impaired sensation due to neuropathy [25], make up one of the main mechanisms of foot ulceration. Nonetheless, it is difficult to stablish whether the biomechanical alterations occur before or after ulceration [21].

1.1.8 Traditional diagnostic methods

There are several diagnostic tools to detect DF but mainly three methods are utilized in consultation. The first one is the Semmes-Weinstein monofilament as shown in figure 1.1, which consists in a nylon filament used to apply pressure on four spots of each foot. The test is considered positive if at least one spot is insensitive [10][12]. Moreover, it has sensitivity values ranging from 66% to 91% and specificity oscillating between 23-86% [4][12].The second method is the tuning fork as shown in figure 1.2, which is used to test vibration sensation and consists of an acoustic resonator operating at 128 Hz applied on the bony prominence of the first toe [4][10]. Also, it presents a sensitivity value of 53%. The last one is the ankle-brachial pressure index, which is obtained from dividing the arterial systolic pressure (ASP) of each ankle and the highest ASP of any brachial artery [12]. Comparing the first and last methods, it can be said that the turning fork is less predictive than the monofilament method [4].

Figure 1.1. Semmes-Weinstein evaluation of the foot. From [26].

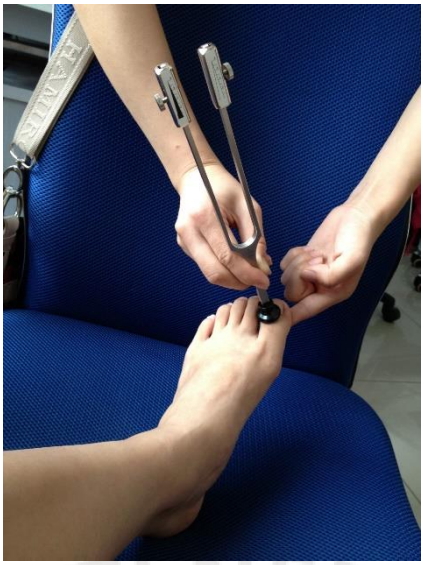

Figure 1.2. Evaluation of a foot with a turning fork. From [27].

1.1.9 Importance of early diagnosis of the diabetic foot

An early diagnosis can improve the incidence of diabetic complications [8].Furthermore, it can have an effect in decreasing the morbidity of the DF [20]. This is exemplified as up to 80% of amputations could be avoided with proper management and implementation of prevention methods [21]. On the other hand, the traditional diagnostic methods mentioned in section 1.1.8 either have sensitivity and specificity values that vary too much over a broad margin or have low sensitivity values. Furthermore, the existence of alternatives that offer quantitative information make impractical the utilization of methods partially relying on subjectivity [13]. In this context, it is important to assess the skin as it pertains to DFU evaluation because as ulceration develops, the skin, loses elasticity and gets stiffer [12][20][23]. Furthermore, there are studies that show that it is possible to characterize elastic properties of skin using elastography [28]. Therefore, elastography may be a viable alternative to assess this condition.

1.2 Elastography Review

1.2.1 Generalities

Elastography imaging refers to a group of techniques that yield a non-invasive assessment of tissue mechanical properties [29]. It was first described in the late 1980's and it has been further developed to provide quantitative evaluations [29][30]. Elastography is founded on the premise that healthy and pathological tissue differ on their respective elasticity values. Therefore, several elastographic techniques can be implemented to differentiate abnormal from healthy

tissue [29][31]. It can be performed mainly through ultrasound elastography (USE) and magnetic resonance elastography (MRE) [32]. Both approaches have an edge over tomography imaging as they do not utilize ionizing radiation for image acquisition purposes. Furthermore, elastography combined with conventional B-mode ultrasound imaging, provides an improved diagnostic performance [33] and is more reliable than traditional procedures such as palpation [34]. Therefore, a more thorough comparison will be made in the following section.

1.2.2 Ultrasound elastography and magnetic resonance elastography

Table 1.2. Comparison of USE and MRE.

Ultrasound		**Magnetic Resonance**	
Advantages	**Disadvantages**	**Advantages**	**Disadvantages**
Wide availability [29]	Low accuracy at high frequencies [35]	Excellent accuracy [32]	Requires a MR unit [32]
Relatively low cost [29]	Depth limitations (in vivo) [35]	Can measure all displacement components [30]	Costly technique [30]
Versatility [29]	-	-	Long acquisition times [36]

Table 1.2 summarizes the advantages and disadvantages of US and MRE implementations. Although MRE is a better technique as it pertains to the accuracy of measurements, US is easier to utilize given that the equipment is portable and considerably smaller. Furthermore, the relatively low cost makes it available to a broader group of people. Therefore, this research will be based on ultrasound elastography.

1.2.3 Classification of US techniques

Elastographic techniques can be classified depending upon the type of information they provide, qualitative or quantitative; the type of excitation force applied, quasi static, transient or harmonic [37]; or the nature of the measurement they make, strain elastography (SE) or shear wave imaging (SWI) [33]. Quantitative data has an advantage over qualitative data because it offers additional information that enables a more accurate classification and

differentiation of tissue, reducing the false positive ratio [34]. Harmonic excitation relies on an external mechanical vibration [38]. On the other hand, quasi static force is applied via external compression through manually applied stress [38] and consequently yields a qualitative measurement [29]. Transient elastography has the need for a dedicated device, does not allows B-mode orientation and presents operator and patient variability [32]. Hence, it can be inferred that harmonic excitation is more advantageous than elastography relying on quasi static or transient force. Finally, strain elastography measures displacements before and after a manual compression has been applied, but assumes uniform stress distribution, which is usually not the case, so it provides a qualitative measurement [29][30]. Also, it is hard to compress deep organs [30].

1.2.4 Shear wave elastography modalities

Particular interest has been put in shear wave elastography, as shear wave speed is directly linked to tissue stiffness through the elasticity modulus [29][39]. Furthermore, shear waves travel at approximately 1-10 m/s in soft tissue while longitudinal waves travel at 1540 m/s, so the relative differences in wave speed found in different tissues are much simpler to contrast [29]. Among the SWE modalities, we have Crawling Waves Sonoelastography (CWS) [30], Reverberant Shear Wave Elastography (RSWE) [39][40], Single Tracking Location Shear Wave Elastography (STL-SWE) [41], Shear Wave Elastography (SWE) [35], among others. Analysis will continue the first three.

1.2.5 Related works

Saavedra *et al.* emphasized the importance of measurement of Surface Acoustic Waves (SAW) in skin because they exist at the top part of an elastic solid [37]. Not doing so, will result in biased estimates; therefore, a compensation factor must be considered [28]. Another interesting fact is that in the work of Cortela *et al.* e difficulty in the measurement of SWS is presented in the DF due to the low depth of tissue [42]. Furthermore, Saavedra assessed skin elasticity in vivo utilizing the CWE technique, but reported the interference pattern was not properly built for frequencies ranges of 300-500 Hz and attributed it to dermis attenuation and boundary reflections [28].

On a related note, CWS is a promising technique that can overcome depth limitations; however, the most prominent techniques of image reconstruction report high variance and the presence of artifacts [34][36]. Moreover, STL-SWE is susceptible to depth attenuation [43]. In that context, Ormachea *et al.* made a comparison of STL-SWE and CWE for estimation of SWS

[41]. However, they assumed plane wave propagation behavior to obtain SWS vs frequency data. Crawling waves are not highly susceptible to aberration, as they only showed a 3% variance; nevertheless, aberration increases in *in vivo* implementations with multiple tissue layers [44][45].

Moreover, limited elastography studies pertaining diabetic foot have been reported since the late 1990's. Most of these studies have been made with MRI where they report stiffer fat pads in diabetic subjects [46]. Additionally, Gefen *et al.* reports that the first metatarsal head is substantially stiffer than other regions [47]. These results follow the trend of expecting stiffer pathological tissue. In ultrasound studies, Naemi *et al.* reported lower relative heal pad stiffness in ulcerated patients in comparison with non-ulcerated ones [19]. These are conflicting results, given that one would expect the exact opposite.

1.3 Justification

Ultrasound elastography has been implemented mainly in the evaluation of liver, thyroid, breast, kidney and prostate [29][35], and no significant work has been done in evaluation of the diabetic foot.

The papers discussed in section 2.4 either reported difficulties in CWS at higher frequencies, reported high variance and artifact presence, assumed plane wave propagation for data acquisition or reported aberration increases with frequency.

Two of the most critical issues with existing techniques had been the assumption of unidirectional wave propagation and plane wave behavior. Such conditions are rarely met in implementations *in vivo* due to internal organ reflections and inhomogeneities. Therefore, Parker *et al.* [39][40] developed the RSWE technique to take advantage of waves propagating in all directions. This implementation would take advantage and exploit these previously adverse conditions because they aid in the formation of the reverberant field.

This approach offers facile implementation and real time image acquisition, which are important conditions for real clinical applications [40].

Finally, del Castillo *et al.* [12] reported the importance of assessing the skin as it pertains to DFU evaluation because as ulceration develops, the skin loses elasticity and gets stiffer. Therefore, we could take advantage of this skin proximity to the bone in order to aid in the reverberation of the waves and estimate its elasticity value.

1.4 Objectives

1.4.1 General objective

- Characterize the elasticity of the foot plant with the novel reverberant shear wave elastography method to assess its feasibility for clinical application.

1.4.2 Specific objectives

- Validate the RSWE method by processing simulated data mimicking wave propagation inside a medium.
- Assess the method on three viscoelastic homogenous phantoms with different gelatin concentrations.
- Apply the method on a small population of healthy and diabetic volunteers and compare the results.

Chapter 2

2 Reverberant Shear Wave Elastography Theoretical Framework

2.1 Introduction

The previous chapter described how diabetes changes the biomechanical properties of tissue, particularly the foot. Furthermore, existing techniques for evaluating ulceration of the foot were stated and briefly described. However, given their inconsistent sensitivity and specificity values, the necessity of another potentially viable alternative was established. Therefore, elastography was brought up as this potential alternative for predicting foot ulceration because it can provide quantitative information and aid a doctor to improve his diagnosis. Moreover, the comparison of this technique and the crawling waves technique was presented as the purpose of this study.

The present chapter elaborates on the necessary concepts to understand the fundamentals of the reverberant shear wave elastography approach. These concepts comprise acoustics, mechanical deformations and advanced vector calculus that explain the formation and usefulness of an ideally diffuse, statistically isotropic reverberant field. Finally, the solution model is presented.

2.2 Theoretical Framework

2.2.1 Acoustic Impedance

Acoustic impedance (z) describes the opposition of an acoustic medium (or inertia) to the propagation of sound waves [48]. It relates a driving force (pressure) and the response this force has in the system (volume flow). The specific acoustic impedance is the ratio between acoustic pressure and the velocity of an oscillating particle [49]. Equation 2.1 governs the acoustic impedance model.

$$z = \rho \cdot c \qquad (2.1)$$

Where z is the acoustic impedance, ρ is the medium density (kg/m^3) and c is the air velocity (m/s).

2.2.2 Plane Wave Compounding

Plane wave compounding allow image acquisition with significantly higher frame rates which has opened the door for important advances in ultrasound imaging by enabling new applications [50]. This is achieved by forming an entire frame from a single acoustic pulse whereas conventional approaches are limited by the number of scan lines used [50]. Compounding solves the issue with merely utilizing plane waves where the beamforming focus is limited to the receive mode: adding the backscattered echoes from the insonified medium in a coherent way leads to improved image resolution [50]. Conversely, adding them in an incoherent way would improve image speckle. The benefits of this method are an increase in contrast, reduction of artifacts, among others [50]. The inconvenience would be that it requires the equipment to possess a high degree of computing power and parallel processing capabilities. A more thorough explanation and a description of the mathematics behind it can be found in [50].

2.2.3 Shear Waves Theory

2.2.3.1 Hooke's Law

Assuming a material is entirely elastic and has no time dependency deformation, meaning the material has no viscosity, Hooke's law, as shown in (2.1), can describe its elastic behavior [29].

$$\sigma = \Gamma \cdot \varepsilon \qquad (2.1)$$

Where σ is stress (Pa), ε is strain (dimensionless) and Γ is the elasticity modulus (Pa).

2.2.3.2 Types of deformational forces

An object can present longitudinal, volume or shear deformation. Longitudinal deformation happens when a pair of forces are either inwards (compression) or outwards (traction) and their direction is perpendicular to the surface. Volume deformation happens when forces compress an object inciting from every direction; the very name conveys that in this type there is a change in volume. For instance, this happens when an object is submerged underwater. Finally, shear deformation happens when a pair of forces incise tangentially to the surface. Since Hooke's law characterizes all these phenomena, the elasticity modulus becomes the Young's modulus

(E) for the first case, the Bulk modulus *(K)* for the second and Shear modulus *(G)* for the last one.

2.2.3.3 Relation between wave speed and elasticity modulus

$$c = \sqrt{\frac{\Gamma}{\rho}} \tag{2.2}$$

Equation (2.2) describes the relation between c and Γ. Since the interest of these study is in shear wave speed (c_s), the previous equation turns into Equation (2.3), where Γ becomes G.

$$c_s = \sqrt{\frac{G}{\rho}} \tag{2.3}$$

Furthermore, it is necessary to know that the previous mentioned types of deformation are not independent from one another. In fact, shear and longitudinal deformation are related through Poisson's ratio (v) [29].

$$E = 2(v + 1) \cdot G \tag{2.4}$$

Given the high content of water of tissue, $v \approx 0.5$. Consequently, combining equation (2.3) and (2.4):

$$E = 3G = 3 \cdot \rho \cdot {c_s}^2 \tag{2.5}$$

Equation (2.5) fully shows the relation between shear wave speed and Young's modulus, which is the one that can characterize tissue elasticity.

2.2.4 Reverberant shear wave elastography theory

2.2.4.1 Summary of the theoretical derivation

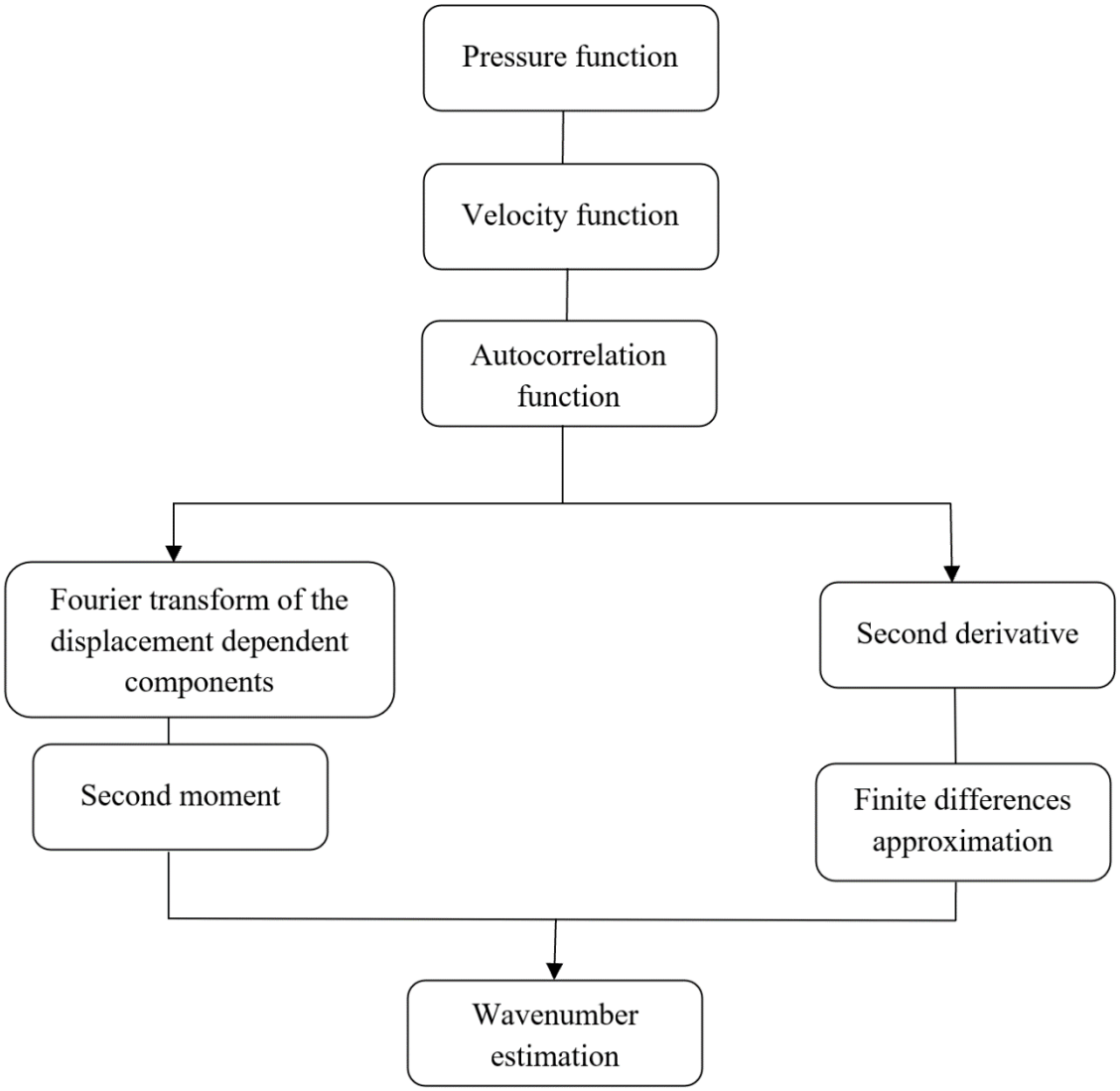

The scheme above summarizes the steps taken to obtain estimators along the axial and lateral components of a travelling shear wave and calculate the wavenumber starting from an expression describing the pressure of a given particle at a given point. The next subsections show some of these steps.

2.2.4.2 Theoretical derivation

The pressure at a given point ε can be assumed as the superposition of waves incident from all directions [39]. Equation (2.6) describes this assumption.

$$\hat{P}(t,\varepsilon) = \sum_{q} \hat{P}_q \cdot e^{j(kn_q\varepsilon - \omega_0 t)} \tag{2.6}$$

$\hat{P}_q$ is the pressure amplitude, k is the wavenumber, n_q is the vector of directional propagation of a given wave at a position ε and ω_0 is the angular frequency. Dividing Eq. 2.6 by the acoustic impedance yields the particle velocity function shown in Eq. 2.7, where n_{ql} is the direction of particle velocity. Note that it is perpendicular to n_q because shear wave particle velocity is normal to its direction of propagation.

$$v_{(t,\varepsilon)} = \frac{\hat{P}(t,\varepsilon)}{\rho \cdot c} = \sum_{q} n_q \hat{v}_q \cdot e^{j(k\boldsymbol{n}_q\varepsilon - \omega_0 t)} \tag{2.7}$$

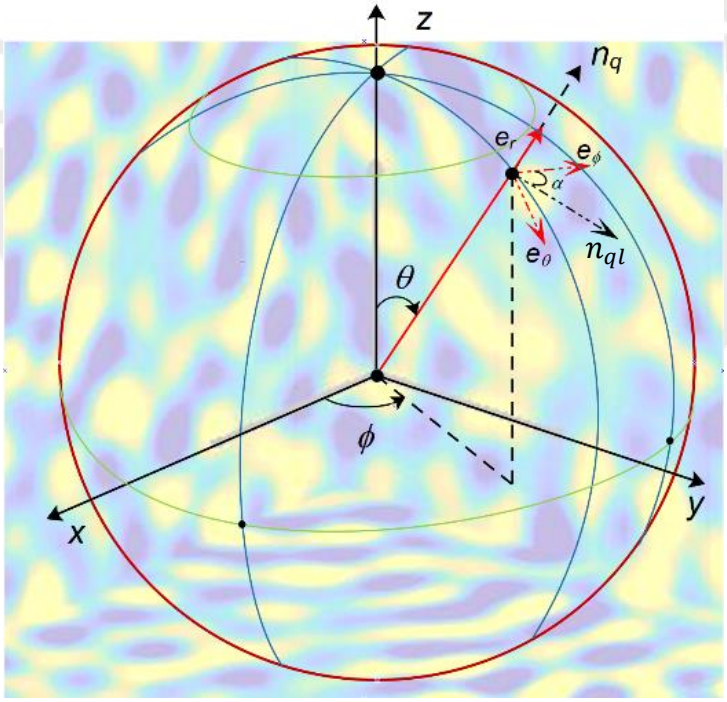

Figure 2.1. Spherical coordinates system showing the azimuth ($\boldsymbol{\phi}$) and elevation ($\boldsymbol{\theta}$) angles. Background: An ideal reverberant shear wave field where shear waves propagate in the interior of an object along $\boldsymbol{4\pi}$ steradians.

Figure 2.1 shows the scenario depicted by the previous equations. Moreover, the summation is understood to be taken over 4π steradians for wave propagation and over 2π for wave particle velocity components at a given point. Also, note that $n_{ql} = \cos(\alpha)e_\phi + \sin(\alpha)e_\theta$, the unit vectors e_ϕ and e_θ are defined as $e_\phi = -\sin(\phi)e_x + \cos(\phi)e_y$ and $e_\theta = \cos(\theta)\cos(\phi)\,e_x + \cos(\theta)\sin(\phi)\,e_y - \sin(\theta)e_z$. The transducer probe is assumed to be aligned with the *x* axis and to detect displacement along the *z* axis. Consequently, it is necessary to project the velocity towards this direction ($n_{zql} = n_{ql} \cdot e_z$) to later calculate the autocorrelation function described in Eq. 2.8.

$$B_{v_z v_{z(\Delta t,\Delta\varepsilon)}} = E\left\{\hat{v}_{z(t,\varepsilon)} \cdot \widehat{v^*}_{z(t+\Delta t,\varepsilon+\Delta\varepsilon)}\right\}$$

$$B_{v_z v_{z(\Delta t,\Delta\varepsilon)}} = E\left\{\left(\sum_q n_{zql}\hat{v}_q \cdot e^{j\left(k\boldsymbol{n_q}\varepsilon-\omega_0 t\right)}\right)\cdot\left(\sum_q n_{zql'}\widehat{v^*}_{q'} \cdot e^{-j\left(kn_{\boldsymbol{q'}}(\varepsilon+\Delta\varepsilon)-\omega_0(t+\Delta t)\right)}\right)\right\}$$

$$\boldsymbol{B_{v_z v_{z(\Delta t,\Delta\varepsilon)}} = E\left\{\left(\sum_q n_{zql}^2 \hat{v}_q^2 \cdot e^{j(\omega_0\Delta t - kn_q\Delta\varepsilon)}\right)\right\}} \qquad (2.8)$$

E represents an ensemble average. Also, note that the average of the summation over discrete directions can be calculated as the average of the summation over all directions because an ideal isotropic diffuse field was assumed. Therefore, the autocorrelation function becomes

$$\boldsymbol{B_{v_x v_{x(\Delta t,\Delta\varepsilon)}} = \frac{V_{avg}{}^2}{4\pi}\iint_{Sphere}\frac{1}{2\pi}\int_0^{2\pi}[-\sin(\theta)\sin(\alpha)]^2\cos\left(\omega_0\Delta t - kn_q\Delta\varepsilon\right)d\alpha d\Omega} \qquad (2.9)$$

$d\Omega$ is the differential solid angle. For particle displacements along the *z* axis,

$$n_q \cdot \Delta\varepsilon_z = \Delta\varepsilon_z \cdot cos(\theta)$$

(2.10)

For particle displacements along the *x* axis,

$$n_q \cdot \Delta\varepsilon_x = \Delta\varepsilon_x \cdot sin(\theta)cos(\phi)$$

(2.11)

Combining Eq. 2.9 & 2.10 and solving the integral:

$$B_{v_z v_{z(\Delta t, \Delta\varepsilon_z)}} = {V_{avg}}^2 cos\,(\omega_0 \Delta t) \cdot \left(\frac{j_1(k\Delta\varepsilon_z)}{k\Delta\varepsilon_z}\right)$$

(2.12)

Likewise, Combining Eq. 2.9 & 2.11 and solving the integral:

$$B_{v_z v_{z(\Delta t, \Delta\varepsilon_x)}} = {V_{avg}}^2 cos\,(\omega_0 \Delta t) \cdot \left(\frac{sin\,(k\Delta\varepsilon_x)}{2k\Delta\varepsilon_x} - \frac{j_1(k\Delta\varepsilon_x)}{2k\Delta\varepsilon_x}\right)$$

(2.13)

j_1 is the spherical Bessel function of the first order of the first kind. Equations 2.12 and 2.13 correspond to the autocorrelation of the particle velocity function for displacements taken along the *z* and *x* directions, respectively. The corresponding equations in [39] are similar, but multiplied by a factor of two. Moreover, they show clear separation of the temporal and spatial components. The spatial components of Eq. 2.12 and 2.13 can be visualized in Figure 2.2.

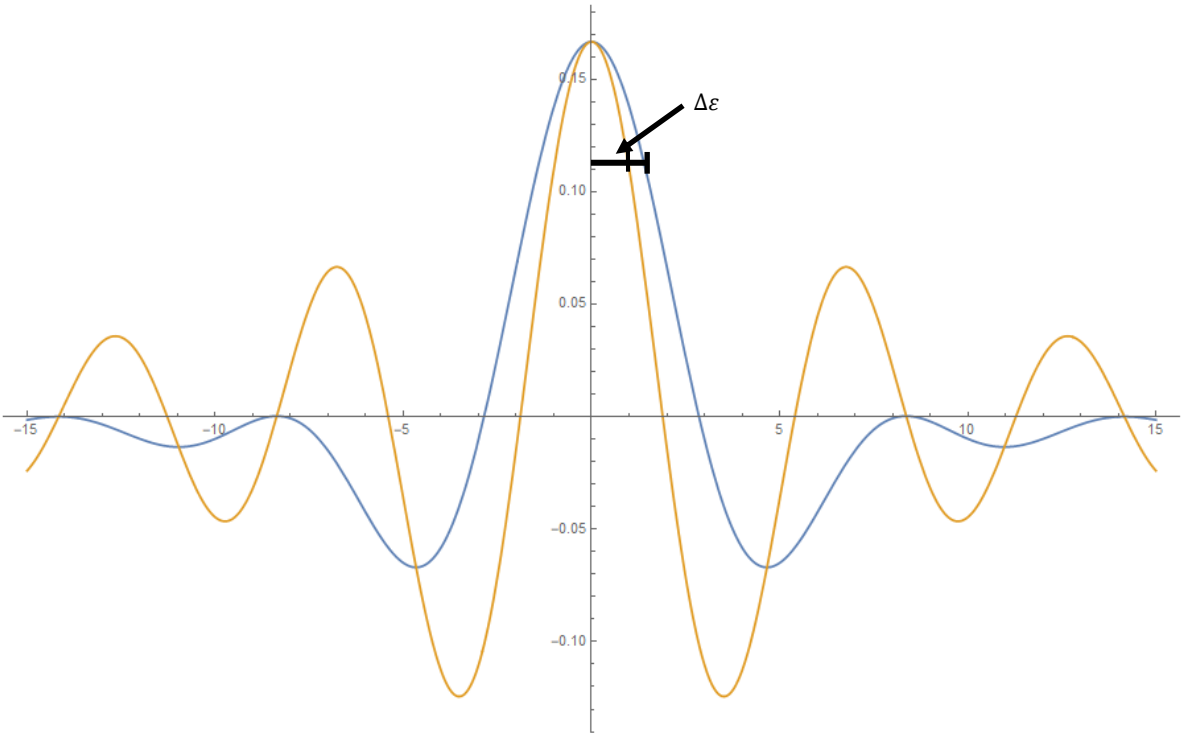

Figure 2.2. Plots of equations 2.12 (blue line) and 2.13 (orange line).

For the next steps, it is necessary to solve for the wavenumber in order to generate the shear wave speed elastogram. The method that is able to perform such task takes a two-step approach. First, second moment of the Fourier transform of the autocorrelation function is taken. This results is equated to the second derivative evaluated at $t = 0$ at some lag $\Delta\varepsilon$ based on the moment and moment generating function relations (the moment generating function resembles the Fourier transform, but this function needs to converge absolutely to exist whereas the Fourier transform allows a more relaxed sense of convergence).

Finally,

$$k_z^2 = \frac{10}{\Delta\varepsilon_z^2 \cdot B_{zv_z}(0)} \cdot \left(Re\{B_{v_z v_z}(0)\} - Re\{B_{v_z v_z}(\Delta\varepsilon_z)\}\right) \tag{2.14}$$

And

$$k_x^2 = \frac{5}{\Delta\varepsilon_x^2 \cdot B_{v_z v_z}(0)} \cdot \left(Re\{B_{v_z v_z}(0)\} - Re\{B_{v_z v_z}(\Delta\varepsilon_x)\}\right) \quad (2.15)$$

Equation 2.14 is the same as the one suggested in [39] whereas Eq. 2.15 is scaled by a factor of 0.5. By taking the mean, both relations can yield an average wavenumber based on the particle velocity detected by an ultrasound system, which is generated by an external vibration source or an acoustic radiation force.

A more detailed explanation of the RSWE theory can be found in [51] and [52]. Moreover, [51] presents an updated version of the theoretical derivation, which was originally published in [39], and serves as the main base for the steps presented in this work.

2.3 Solution Model

The flow chart presented below synthetizes the necessary steps to fulfil the objectives of this thesis. The first two steps (1 & 2) involve each of the two specific objectives. The generation of the reverberant field is of paramount importance since it is the base of the method. The "how" of both cases will be specified on the next chapter. Furthermore, the criteria for filtering on each domain and the technique used for creating the image will be detailed. Calculating the elasticity modulus is straight forward considering equation 2.5; however, spatial resolution and contrast will be detailed in the upcoming section.

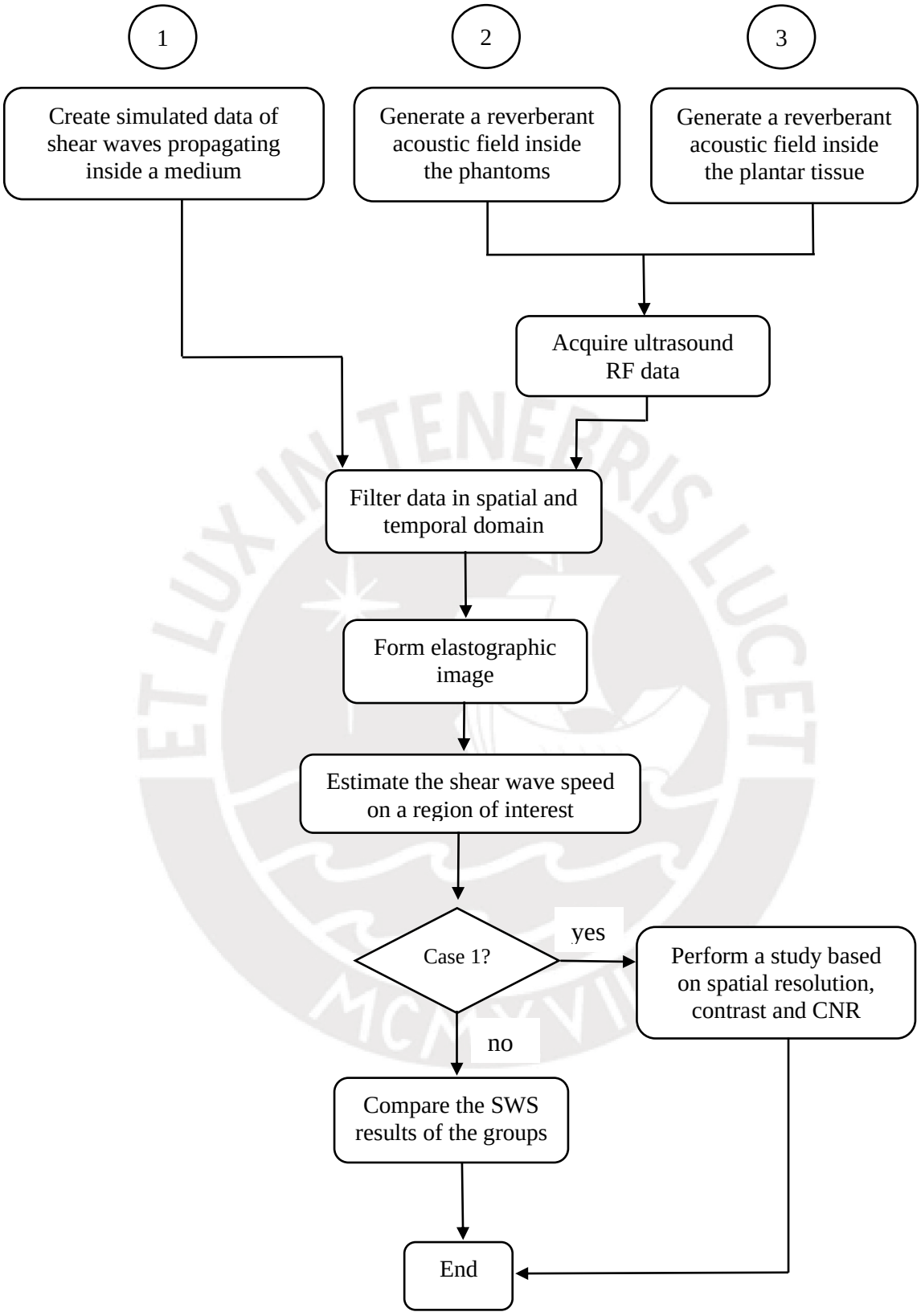
1
2
3
Create simulated data of shear waves propagating inside a medium
Generate a reverberant acoustic field inside the phantoms
Generate a reverberant acoustic field inside the plantar tissue
Acquire ultrasound RF data
Filter data in spatial and temporal domain
Form elastographic image
Estimate the shear wave speed on a region of interest
Case 1?
yes
Perform a study based on spatial resolution, contrast and CNR
no
Compare the SWS results of the groups
End

3 Conclusions

- A need for a quantitative approach that could differentiate foot tissue between a healthy person from one in the process of developing diabetic foot is paramount, given that diabetes is becoming an escalating issue. Then, it could be feasible to implement ultrasound RSWE for that purpose.

- The theoretical derivation of RSWE shows that there are a set of equations that relate wavenumber and wave velocity autocorrelation both in an exact and approximation form. Herein, it is necessary to validate which method would be more appropriate to follow.

- Literature results indicate that the plantar tissue behaves in a viscoelastic manner. Therefore, the methodology should include experiments implementing RSWE corroborating such behavior in gelatin phantoms.

4 Recommendations and Future Works

- A comparison of tissue stiffness between cohorts of healthy and diabetic volunteers is underway. The methodology for that work is derived from the specific objectives presented in this document.

- It is recommended to always count with the assistance of a medical professional to avoid erroneous acquisitions while working with real tissue, given that even a radiologist experimented issues locating and maintaining the anatomical landmark on screen.

- The optimal number of vibration sources necessary to create a diffuse isotropic reverberant shear wave field has not been found. Purely elastic mediums could require only one source, but phantoms and biological tissue do not behave this way. Therefore, there is a need to compensate for attenuation loses so the optimal number of external vibration sources is still to be investigated.

5 Bibliography

[1] N. H. Cho *et al.*, "IDF Diabetes Atlas: Global estimates of diabetes prevalence for 2017 and projections for 2045," *Diabetes Res. Clin. Pract.*, vol. 138, pp. 271–281, 2018, doi: 10.1016/j.diabres.2018.02.023.

[2] D. Atlas, "International diabetes federation," *IDF Diabetes Atlas, 7th edn. Brussels, Belgium Int. Diabetes Fed.*, 2015.

[3] M. Dansinger, "Types of Diabetes Mellitus," *WebMD*, 2019. https://www.webmd.com/diabetes/guide/types-of-diabetes-mellitus (accessed Mar. 05, 2019).

[4] M. P. Khanolkar, S. C. Bain, and J. W. Stephens, "The diabetic foot," *QJM An Int. J. Med.*, vol. 101, no. 9, pp. 685–695, 2008.

[5] Y. Jiang *et al.*, "Epidemiology of type 2 diabetic foot problems and predictive factors for amputation in china," *Int. J. Low. Extrem. Wounds*, vol. 14, no. 1, pp. 19–27, 2015, doi: 10.1177/1534734614564867.

[6] Ministerio de Salud – Dirección General de Intervenciones Estratégicas en Salud Pública, "Guía de Práctica Clínica para el Diagnóstico, Tratamiento y Control de la Diabetes Mellitus Tipo 2 en el Primer Nivel de Atención," Lima, Perú, 2016.

[7] J. Beagley, L. Guariguata, C. Weil, and A. A. Motala, "Global estimates of undiagnosed diabetes in adults," *Diabetes Res. Clin. Pract.*, vol. 103, no. 2, pp. 150–160, Feb. 2014, doi: 10.1016/J.DIABRES.2013.11.001.

[8] E. W. Gregg, N. Sattar, and M. K. Ali, "The changing face of diabetes complications," *Lancet Diabetes Endocrinol.*, vol. 4, no. 6, pp. 537–547, Jun. 2016, doi: 10.1016/S2213-8587(16)30010-9.

[9] S. Tiwari, D. D. Pratyush, S. K. Gupta, and S. K. Singh, "Significance of Surgical Intervention in the Management of Diabetic Foot Infections," *Microbiol. Surg. Infect.*, pp. 251–266, Jan. 2014, doi: 10.1016/B978-0-12-411629-0.00015-5.

[10] K. Bakker, J. Apelqvist, N. C. Schaper, and I. W. G. on the Diabetic Foot Editorial Board, "Practical guidelines on the management and prevention of the diabetic foot

2011," *Diabetes. Metab. Res. Rev.*, vol. 28, pp. 225–231, 2012.

[11] A. J. M. Boulton, "The diabetic foot," *Medicine (United Kingdom)*, vol. 47, no. 2. Elsevier, pp. 100–105, Feb. 01, 2019, doi: 10.1016/j.mpmed.2018.11.001.

[12] R. A. Del Castillo, J. A. Fernández, and F. J. Del Castillo, "Guía de práctica clínica en el pie diabético," *Arch. Med.*, vol. 10, no. 1, pp. 1–17, 2014, doi: 10.3823/1211.

[13] J. J. V. Netten, D. Clark, P. A. Lazzarini, M. Janda, and L. F. Reed, "The validity and reliability of remote diabetic foot ulcer assessment using mobile phone images," *Sci. Rep.*, vol. 7, no. 1, pp. 1–10, 2017, doi: 10.1038/s41598-017-09828-4.

[14] P. Zhang, J. Lu, Y. Jing, S. Tang, D. Zhu, and Y. Bi, "Global epidemiology of diabetic foot ulceration: a systematic review and meta-analysis †," *Ann. Med.*, vol. 49, no. 2, pp. 106–116, 2017, doi: 10.1080/07853890.2016.1231932.

[15] K. Heyer, K. Herberger, K. Protz, G. Glaeske, and M. Augustin, "Epidemiology of chronic wounds in Germany: Analysis of statutory health insurance data," *Wound Repair Regen.*, vol. 24, no. 2, pp. 434–442, 2016, doi: 10.1111/wrr.12387.

[16] M. M. Ţânţu *et al.*, "Diabetic foot – Epidemiological and histopathological aspects," *Rom. J. Morphol. Embryol.*, vol. 59, no. 3, pp. 895–902, 2018.

[17] A. O. Almobarak, H. Awadalla, M. Osman, and M. H. Ahmed, "Prevalence of diabetic foot ulceration and associated risk factors: an old and still major public health problem in Khartoum, Sudan?," *Ann. Transl. Med.*, vol. 5, no. 17, 2017.

[18] N. D. Cucho and A. Alarcon, "Diseño e implementación de una plantilla para la medición de presión plantar para la prevención de ulceraciones en la patología de pie diabético," PONTIFICIA UNIVERSIDAD CATÓLICA DEL PERÚ, 2012.

[19] R. Naemi, P. Chatzistergos, L. Sundar, N. Chockalingam, and A. Ramachandran, "Differences in the mechanical characteristics of plantar soft tissue between ulcerated and non-ulcerated foot," *J. Diabetes Complications*, vol. 30, no. 7, pp. 1293–1299, 2016, doi: 10.1016/j.jdiacomp.2016.06.003.

[20] H. M. Rathur and A. J. M. Boulton, "The neuropathic diabetic foot," *Nat. Clin. Pract. Endocrinol. Metab.*, vol. 3, no. 1, pp. 14–25, 2007, doi: 10.1038/ncpendmet0347.

[21] R. Naemi, P. Chatzistergos, S. Suresh, L. Sundar, N. Chockalingam, and A.

Ramachandran, “Can plantar soft tissue mechanics enhance prognosis of diabetic foot ulcer?,” *Diabetes Res. Clin. Pract.*, vol. 126, pp. 182–191, 2017, doi: 10.1016/j.diabres.2017.02.002.

[22] Y. N. Wang, K. Lee, J. B. Shofer, and W. R. Ledoux, “Histomorphological and biochemical properties of plantar soft tissue in diabetes,” *Foot*, vol. 33, pp. 1–6, 2017, doi: 10.1016/j.foot.2017.06.001.

[23] W. R. Ledoux, S. Pai, J. B. Shofer, and Y. N. Wang, “The association between mechanical and biochemical/histological characteristics in diabetic and non-diabetic plantar soft tissue,” *J. Biomech.*, vol. 49, no. 14, pp. 3328–3333, 2016, doi: 10.1016/j.jbiomech.2016.08.021.

[24] S. Pai and W. R. Ledoux, “The compressive mechanical properties of diabetic and non-diabetic plantar soft tissue,” *J. Biomech.*, vol. 43, no. 9, pp. 1754–1760, Jun. 2010, doi: 10.1016/J.JBIOMECH.2010.02.021.

[25] P. E. Chatzistergos, R. Naemi, L. Sundar, A. Ramachandran, and N. Chockalingam, “The relationship between the mechanical properties of heel-pad and common clinical measures associated with foot ulcers in patients with diabetes,” *J. Diabetes Complications*, vol. 28, no. 4, pp. 488–493, 2014, doi: 10.1016/j.jdiacomp.2014.03.011.

[26] OPC Health, “Touch Test Evaluator,” *Sensory Assessment & Training*, 2019. https://www.opchealth.com.au/touch-test-sensory-evaluator (accessed May 24, 2019).

[27] J. Zhang, “Rapid Screening for Diabetic Neuropathy Using the 128-Hz Vibration Tuning Fork,” *Alibaba*. https://www.alibaba.com/product-detail/Rapid-Screening-for-Diabetic-Neuropathy-Using_1628177886.html (accessed May 24, 2019).

[28] A. C. Saavedra, J. Arroyo, F. Zvietcovich, R. J. Lavarello, and B. Castaneda, “In vivo estimation of the Young’s modulus in normal human dermis,” *Proc. Annu. Int. Conf. IEEE Eng. Med. Biol. Soc. EMBS*, vol. 2018-July, pp. 3456–3459, 2018, doi: 10.1109/EMBC.2018.8512935.

[29] R. M. S. Sigrist, J. Liau, A. El Kaffas, M. C. Chammas, and J. K. Willmann, “Ultrasound elastography: Review of techniques and clinical applications,” *Theranostics*, vol. 7, no. 5, pp. 1303–1329, 2017, doi: 10.7150/thno.18650.

[30] K. J. Parker, M. M. Doyley, and D. J. Rubens, “Corrigendum: Imaging the elastic

properties of tissue: the 20 year perspective," *Phys. Med. Biol.*, vol. 57, no. 16, pp. 5359–5360, 2012, doi: 10.1088/0031-9155/57/16/5359.

[31] B. Castaneda, J. Ormachea, P. Rodriguez, and K. J. Parker, "Application of numerical methods to elasticity imaging," *Mol Cell Biomech*, vol. 10, no. 1, pp. 43–65, 2013.

[32] M. Friedrich-Rust, T. Poynard, and L. Castera, "Critical comparison of elastography methods to assess chronic liver disease," *Nat. Rev. Gastroenterol. Hepatol.*, vol. 13, no. 7, pp. 402–411, 2016, doi: 10.1038/nrgastro.2016.86.

[33] H. J. Kim *et al.*, "Comparison of strain and shear wave elastography for qualitative and quantitative assessment of breast masses in the same population," *Sci. Rep.*, vol. 8, no. 1, pp. 1–11, 2018, doi: 10.1038/s41598-018-24377-0.

[34] E. González, P. Li, J. Ormachea, K. Parker, R. Lavarello, and B. Castañeda, "Regularized wavelength average velocity estimator for quantitative ultrasound elastography," *IEEE Int. Ultrason. Symp. IUS*, vol. 2016-Novem, pp. 0–3, 2016, doi: 10.1109/ULTSYM.2016.7728691.

[35] M. W. Urban, J. Chen, and R. L. Ehman, "Comparison of shear velocity dispersion in viscoelastic phantoms measured by ultrasound-based shear wave elastography and magnetic resonance elastography," *IEEE Int. Ultrason. Symp. IUS*, pp. 0–3, 2017, doi: 10.1109/ULTSYM.2017.8092418.

[36] E. A. Gonzalez, S. E. Romero, and B. Castaneda, "Real Time Crawling Wave Sonoelastography for human muscle characterization: Initial results," *IEEE Trans. Ultrason. Ferroelectr. Freq. Control*, vol. 66, no. 3, pp. 563–571, 2018, doi: 10.1109/TUFFC.2018.2858658.

[37] A. C. Saavedra, F. Zvietcovich, R. J. Lavarello, and B. Castaneda, "Measurement of surface acoustic waves in high-frequency ultrasound: Preliminary results," *Proc. Annu. Int. Conf. IEEE Eng. Med. Biol. Soc. EMBS*, pp. 3000–3003, 2017, doi: 10.1109/EMBC.2017.8037488.

[38] A. C. Saavedra Bazan, "COMPARACIÓN DE TÉCNICAS DE ELASTOGRAFÍA CUANTITATIVA BASADAS EN VIBRACIÓN MECÁNICA EXTERNA EN EQUIPOS ULTRASÓNICOS DE INVESTIGACIÓN CON DIFERENTES RANGOS DE FRECUENCIA," Pontificia Universidad Católica del Perú, 2015.

[39] K. J. Parker, J. Ormachea, F. Zvietcovich, and B. Castaneda, “Reverberant shear wave fields and estimation of tissue properties,” *Phys. Med. Biol.*, vol. 62, no. 3, pp. 1046–1061, 2017, doi: 10.1088/1361-6560/aa5201.

[40] J. Ormachea, B. Castaneda, and K. J. Parker, “Shear Wave Speed Estimation Using Reverberant Shear Wave Fields: Implementation and Feasibility Studies,” *Ultrasound Med. Biol.*, vol. 44, no. 5, pp. 963–977, 2018, doi: 10.1016/j.ultrasmedbio.2018.01.011.

[41] J. Ormachea, R. J. Lavarello, S. A. McAleavey, K. J. Parker, and B. Castaneda, “Shear Wave Speed Measurements Using Crawling Wave Sonoelastography and Single Tracking Location Shear Wave Elasticity Imaging for Tissue Characterization,” *IEEE Trans. Ultrason. Ferroelectr. Freq. Control*, vol. 63, no. 9, pp. 1351–1360, 2016, doi: 10.1109/TUFFC.2016.2576962.

[42] G. Cortela, L. Leija, A. Vera, N. Benech, and C. Negreira, “Elastograms of the diabetic foot by ultrasonic impulse elastography,” *2016 Glob. Med. Eng. Phys. Exch. Am. Heal. Care Exch. GMEPE/PAHCE 2016*, pp. 1–4, 2016, doi: 10.1109/GMEPE-PAHCE.2016.7504663.

[43] R. Ahmed, S. A. Gerber, S. A. McAleavey, G. Schifitto, and M. M. Doyley, “Plane-wave imaging improves single-track location shear wave elasticity imaging,” *IEEE Trans. Ultrason. Ferroelectr. Freq. Control*, vol. 65, no. 8, pp. 1402–1414, 2018, doi: 10.1109/TUFFC.2018.2842468.

[44] G. Torres, C. Amador, M. Urban, B. Castañeda, and R. Lavarello, “Comparative evaluation of aberration effects in crawling wave sonoelastography and comb-push ultrasound shear elastography,” *IEEE Int. Ultrason. Symp. IUS*, vol. 2016-Novem, no. x, pp. 1–4, 2016, doi: 10.1109/ULTSYM.2016.7728733.

[45] G. Torres, K. J. Parker, B. Castaneda, and R. Lavarello, “Effects of aberration in crawling wave sonoelastography,” *2015 IEEE Int. Ultrason. Symp. IUS 2015*, pp. 2–5, 2015, doi: 10.1109/ULTSYM.2015.0380.

[46] Y. Y. Cheung *et al.*, “Magnetic Resonance Elastography of the Plantar Pads,” vol. 30, no. 2, pp. 1–6, 2006, [Online]. Available: papers3://publication/uuid/AB363473-8C69-430E-AE50-9BA05EEF0D30.

[47] A. Gefen, M. Megido-Ravid, M. Azariah, Y. Itzchak, and M. Arcan, “Integration of

plantar soft tissue stiffness measurements in routine MRI of the diabetic foot," *Clin. Biomech.*, vol. 16, no. 10, pp. 921–925, Dec. 2001, doi: 10.1016/S0268-0033(01)00074-2.

[48] "impedancia acústica," *Real Academia de Ingeniería*. http://diccionario.raing.es/es/lema/impedancia-acústica (accessed May 20, 2019).

[49] Acustipedia, "¿Qué es la impedancia acústica?," *Inercoacustica*, 2012. http://www.inercoacustica.com/acustipedia/item/216-¿qué-es-la-impedancia-acústica? (accessed May 20, 2019).

[50] G. Montaldo, M. Tanter, J. Bercoff, N. Benech, and M. Fink, "Coherent plane-wave compounding for very high frame rate ultrasonography and transient elastography," *IEEE Trans. Ultrason. Ferroelectr. Freq. Control*, vol. 56, no. 3, pp. 489–506, 2009.

[51] J. Ormachea, "Viscoelastic Tissue Characterization Based on Harmonic and Transient ShearWave Elastography," University of Rochester, Rochester, New York, 2020.

[52] F. Zvietcovich, P. Pongchalee, P. Meemon, J. P. Rolland, and K. J. Parker, "Reverberant 3D optical coherence elastography maps the elasticity of individual corneal layers," *Nat. Commun.*, vol. 10, no. 1, pp. 1–13, 2019.